Differential Expression of Glucose Transporters and Hexokinases in Prostate Cancer with a Neuroendocrine Gene Signature: A Mechanistic Perspective for ^{18}F-FDG Imaging of PSMA-Suppressed Tumors

Martin K. Bakht[1–3], Jessica M. Lovnicki[4], Janice Tubman[1], Keith F. Stringer[1,5], Jonathan Chiaramonte[6], Michael R. Reynolds[6], Iulian Derecichei[1], Rosa-Maria Ferraiuolo[7], Bre-Anne Fifield[1], Dorota Lubanska[1], So Won Oh[2,3], Gi Jeong Cheon[2,3], Cheol Kwak[8], Chang Wook Jeong[8], Keon Wook Kang[2,3], John F. Trant[6], Colm Morrissey[9], Ilsa M. Coleman[10], Yuzhuo Wang[4], Hojjat Ahmadzadehfar[11], Xuesen Dong[4], and Lisa A. Porter[1]

[1]Department of Biomedical Sciences, University of Windsor, Windsor, Ontario, Canada; [2]Department of Nuclear Medicine, Seoul National University College of Medicine, Seoul, Korea; [3]Laboratory of Molecular Imaging and Therapy, Cancer Research Institute, Seoul National University College of Medicine, Seoul, Korea; [4]Vancouver Prostate Centre, Department of Urologic Sciences, University of British Columbia, Vancouver, British Columbia, Canada; [5]Department of Pathology, Cincinnati Children's Hospital Medical Center, Cincinnati, Ohio; [6]Department of Chemistry and Biochemistry, University of Windsor, Windsor, Ontario, Canada; [7]Barbara Ann Karmanos Cancer Institute, Detroit, Michigan; [8]Department of Urology, Seoul National University College of Medicine, Seoul, Korea; [9]Department of Urology, University of Washington, Seattle, Washington; [10]Divison of Human Biology, Fred Hutchinson Cancer Research Center, Seattle, Washington; and [11]Department of Nuclear Medicine, University Hospital Bonn, Bonn, Germany

Although the incidence of de novo neuroendocrine prostate cancer (PC) is rare, recent data suggest that low expression of prostate-specific membrane antigen (PSMA) is associated with a spectrum of neuroendocrine hallmarks and androgen receptor (AR) suppression in PC. Previous clinical reports indicate that PCs with a phenotype similar to neuroendocrine tumors can be more amenable to imaging by ^{18}F-FDG than by PSMA-targeting radioligands. In this study, we evaluated the association between neuroendocrine gene signature and ^{18}F-FDG uptake–associated genes including glucose transporters (GLUTs) and hexokinases, with the goal of providing a genomic signature to explain the reported ^{18}F-FDG avidity of PSMA-suppressed tumors. **Methods:** Data-mining approaches, cell lines, and patient-derived xenograft models were used to study the levels of 14 members of the *SLC2A* family (encoding GLUT proteins), 4 members of the hexokinase family (genes *HK1–HK3* and *GCK*), and PSMA (*FOLH1* gene) after AR inhibition and in correlation with neuroendocrine hallmarks. Also, we characterize a neuroendocrine-like PC (NELPC) subset among a cohort of primary and metastatic PC samples with no neuroendocrine histopathology. We measured glucose uptake in a neuroendocrine-induced in vitro model and a zebrafish model by nonradioactive imaging of glucose uptake using a fluorescent glucose bioprobe, GB2-Cy3. **Results:** This work demonstrated that a neuroendocrine gene signature associates with differential expression of genes encoding GLUT and hexokinase proteins. In NELPC, elevated expression of *GCK* (encoding glucokinase protein) and decreased expression of *SLC2A12* correlated with earlier biochemical recurrence. In tumors treated with AR inhibitors, high expression of *GCK* and low expression of *SLC2A12* correlated with neuroendocrine histopathology and PSMA gene suppression. GLUT12 suppression and upregulation of glucokinase were observed in neuroendocrine-induced PC cell lines and patient-derived xenograft models. A higher glucose uptake was confirmed in low-PSMA tumors using a GB2-Cy3 probe in a zebrafish model. **Conclusion:** A neuroendocrine gene signature in neuroendocrine PC and NELPC associates with a distinct transcriptional profile of GLUTs and hexokinases. PSMA suppression correlates with GLUT12 suppression and glucokinase upregulation. Alteration of ^{18}F-FDG uptake–associated genes correlated positively with higher glucose uptake in AR- and PSMA-suppressed tumors. Zebrafish xenograft tumor models are an accurate and efficient preclinical method for monitoring nonradioactive glucose uptake.

Key Words: neuroendocrine PC; PSMA; glucose transporters; hexokinases, glucokinase

J Nucl Med 2020; 61:904–910
DOI: 10.2967/jnumed.119.231068

The androgen receptor (AR) plays a central role in regulating the transcriptional events driving prostate cancer (PC) progression and development of metastatic castration-resistant PC (mCRPC) (*1*). AR inhibition is an effective therapeutic approach for most patients at different stages of PC. Although the incidence of de novo neuroendocrine PC (NEPC) is considered rare, several emerging forms of PC with low levels of AR are identified. The suppression and low activity of AR in these patients is largely associated with a neuroendocrine gene signature (NEGS) and resistance to AR inhibition (*2,3*).

AR-directed therapy of mCRPC could promote cellular plasticity and development of an AR-suppressed phenotype similar to

Received Jun. 2, 2019; revision accepted Oct. 22, 2019.
For correspondence or reprints contact either of the following:
Gi Jeong Cheon, Department of Nuclear Medicine, Seoul National University College of Medicine, Seoul 110-744, Korea.
E-mail: larrycheon@snu.ac.kr
Lisa A. Porter, Department of Biomedical Sciences, University of Windsor, Windsor, N9B 3P4 Ontario, Canada.
E-mail: lporter@uwindsor.ca
Published online Dec. 5, 2019.

NEPC, which manifests the histopathology of neuroendocrine disease (*4*). Another emerging phenotype of mCRPC is AR-null and neuroendocrine-null, classified as double-negative PC (DNPC) (*3*). A recent molecular subtyping of PC patients with no history of AR-directed therapies identified a neuroendocrine-positive subtype with low chromatin binding and activity of AR. These patients have been referred to as having neuroendocrine-like PC (NELPC) since it does not represent the neuroendocrine histopathology (*2,5*). NEPC is associated with the loss of RE1-silencing transcription factor (*REST*) due to alternate splicing by the RNA splicing factor serine/arginine repetitive matrix 4 (*SRRM4*). *SRRM4* plays a crucial role in progression to NEPC under next-generation AR inhibitors, such as abiraterone and enzalutamide (*6*). Hence, the elevation of *SRRM4* and the loss of its target *REST* could be specific markers of treatment-induced NEPC.

AR regulates the expression of *FOLH1* gene encoding the transmembrane protein prostate-specific membrane antigen (PSMA). PSMA-targeted molecular imaging and therapy are transforming the landscape of PC management (*7,8*). Despite the impactful implications of PSMA, there are clinical reports that suggest that PSMA-targeted imaging does not effectively visualize NEPC tumors (*8–10*). Preclinical studies confirmed that the induction of lineage plasticity by AR inhibition leads to neuroendocrine transdifferentiation and suppression of PSMA (*11*).

Similar to glucose, ^{18}F-FDG is actively transported into the cell by the protein family of glucose transporters (GLUTs) and is encoded by *SLC2A* genes, followed by phosphorylation by hexokinase (*12*). In some types of tumors, a positive correlation has been reported between ^{18}F-FDG uptake and the levels of specific GLUTs and hexokinases (*12–14*). ^{18}F-FDG PET is a well-accepted approach for delineation of proliferative and poorly differentiated or dedifferentiated neuroendocrine tumors (*15*). Nevertheless, ^{18}F-FDG PET has been considered ineffective in assessing metastatic tumor burden and monitoring therapy response (*16*). Recent case reports illustrate that NEPC delineation may be more feasible by ^{18}F-FDG than by PSMA radioligands (*17,18*) and Spratt et al. (*19*) demonstrated the utility of ^{18}F-FDG PET for NEPC imaging. Interestingly, Thang et al. (*20*) screened patients with ^{68}Ga-PSMA-11 and ^{18}F-FDG PET, and they identified a subset of patients with low PSMA-radioligand uptake and high ^{18}F-FDG uptake.

Development of nonradioactive glucose analogs enabling delineation of the glucose uptake of tumors has been studied using a variety of optical approaches mostly in mouse models (*21*). PC xenograft studies in zebrafish are coming to the forefront as a cost-effective and time-efficient model for drug screening, and the fluorescent glucose bioprobe GB2-Cy3 has been used to monitor glucose uptake in a zebrafish model (*22,23*). However, the feasibility of monitoring glucose uptake in PC in a zebrafish model has not been evaluated.

In this work we used data-mining approaches, cell lines, and patient-derived xenograft (PDX) models to study the expression levels of glucose uptake–associated genes, including GLUTs and hexokinases in NEPC and NELPC, to provide a genomic rationalization for the previously reported ^{18}F-FDG avidity of PSMA-suppressed PC tumors. We also present the feasibility of nonradioactive in vivo imaging of glucose uptake using a zebrafish model.

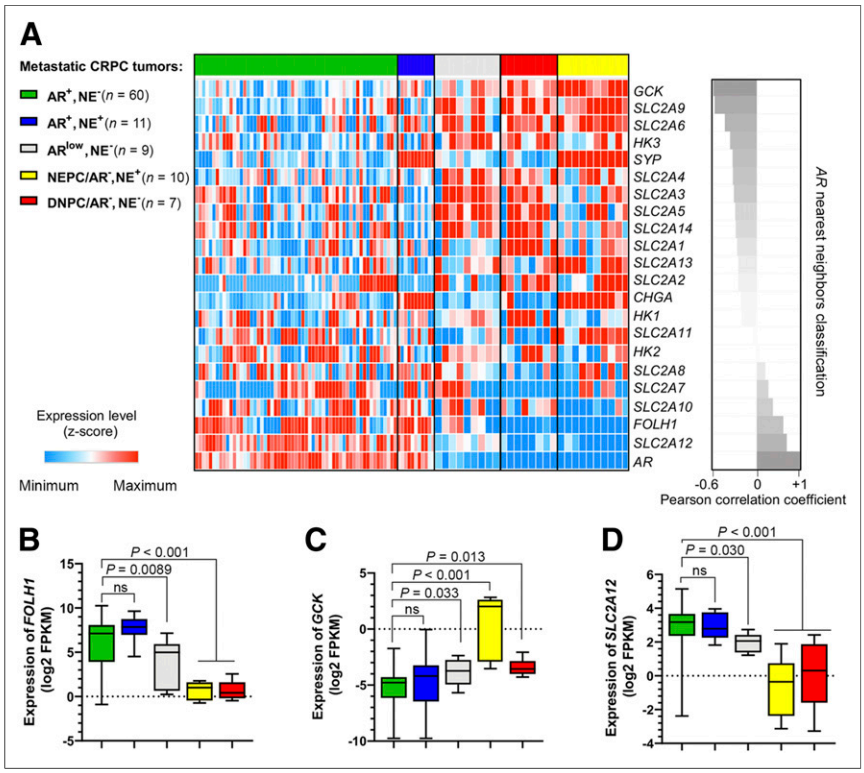

FIGURE 1. AR-negative subsets of mCRPC in UW cohort (*3*) have suppressed expression of *FOLH1* and differential expression of *SLC2A* and hexokinase genes. (A) Heat-map plot of expression levels of *SLC2A* family members, hexokinase genes, AR, *FOLH1,* and neuroendocrine markers sorted on the basis of nearest neighbors clustering to AR. (B, C, and D) Box–whisker plots showing expression of *FOLH1*, *GCK,* and *SLC2A12,* respectively.

MATERIALS AND METHODS

Cell Culture

The LNCaP cell line was purchased from ATCC and grown in RPMI-1640 in the presence of 10% fetal bovine serum. Progression to NEPC was achieved by culturing LNCaP cells in RPMI-1640 medium with 10% charcoal-stripped serum for 4 mo. Under these conditions, cell morphology gradually changed into a mixture of a neuroendocrine-like phenotype and a nonneuroendocrine phenotype. After 4 mo, a subclone with a neuroendocrine-like phenotype was isolated (LNCaP-NEPC). LNCaP cells, maintained in RPMI-1640 plus fetal bovine serum, were used as a control and are referred to as LNCaP-adenocarcinoma PC (AdPC).

Antibodies

The immunoblotting technique used was previously described (*11*). Antibodies are as follows: actin (MAB150-1R; Chemicon-Millipore), PSMA (D4S1F; Cell Signaling), AR (sc-816; Santa Cruz Biotechnology), NSE (sc-271384; Santa Cruz Biotechnology), GCK (sc-17819; Santa Cruz Biotechnology), and GLUT12 (ab100993; Abcam).

Data-Mining Analysis

Using 268 PC samples from 3 different cohorts, we assessed the transcript abundance for all of the *SLC2A* family (*SLC2A1-14*) and the hexokinase family (*HK1–HK4, HK4* referred to as *GCK*). In addition, we

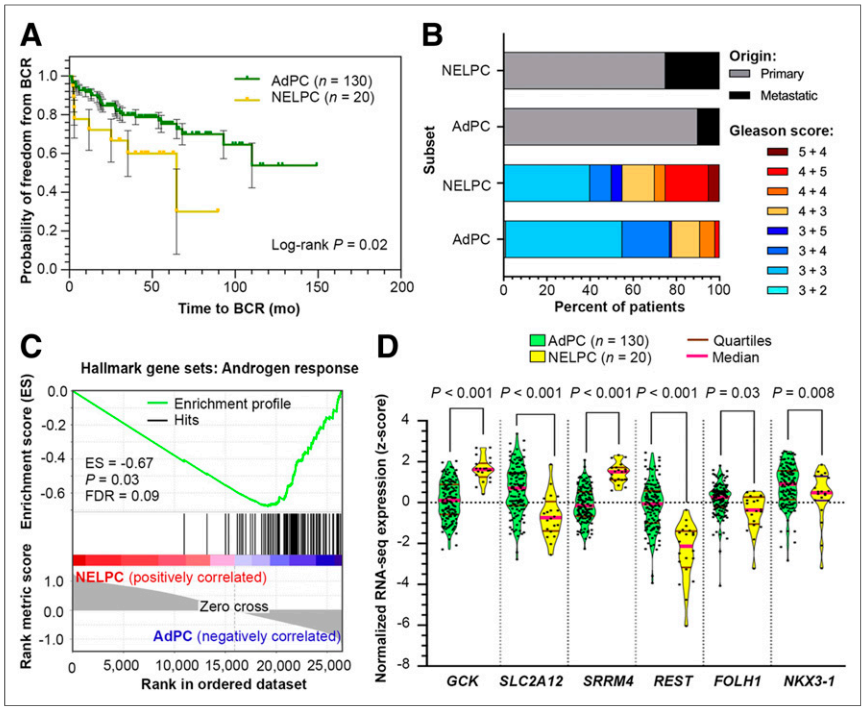

FIGURE 2. NELPC subset of Memorial Sloan Kettering Cancer Center cohort (*24*) displays shorter time to BCR (A), greater prevalence of metastatic and high Gleason score specimens (B), and lack of AR response (C). (D) Violin plots compare distribution of *SLC2A12*, *GCK,* and *FOLH1* expressions in NELPC and AdPC subsets. BCR = biochemical recurrence; ES = enrichment score; FDR = false discovery rate.

monitored the PSMA gene (*FOLH1*), *SRRM4* as a positive marker of treatment-induced NEPC, and *REST* as a negative marker of NEPC. Patients with a lack of NEGS or neuroendocrine histopathology are referred to as AdPC.

To assess the lineage plasticity of mCRPC, samples from a tissue acquisition necropsy platform established at the University of Washington (UW) were used (*3*). All rapid autopsy tissues were collected from patients who gave written informed consent under the aegis of the PC Donor Program at the UW, and the Institutional Review Board of the UW approved this study. We classified our mCRPC subtypes as AdPC (AR-positive/neuroendocrine-negative), AR-suppressed AdPC (low AR/neuroendocrine-negative), NEPC (AR-negative/neuroendocrine-positive), and DNPC (AR-negative/neuroendocrine-negative). In addition, we used the Beltran cohort (*4*) with histologically confirmed mCRPC-AdPC and mCRPC-NEPC samples. We identified a NELPC subset among AdPC tumors from the Memorial Sloan Kettering Cancer Center cohort (*24*) using the meta-signature of prototypical high-grade NEPC (*25*). Gene set enrichment analysis was performed on the identified subsets using gene sets downloaded from the Molecular Signatures Database (*26*).

Mouse PDX Models

Fresh PC tissues from patients were grafted under the kidney capsules of nonobese diabetic or severe combined immunodeficient mice. The Institutional Review Board and Animal Care Committee of the University of British Columbia approved this study, and all subjects gave written informed consent. We previously characterized and validated these models (*27*).

GB2-Cy3 Synthesis and Cellular Uptake

Synthesis and in vitro uptake of a glucose bioprobe, GB2-Cy3, were previously reported with some modifications (*22,28,29*). Full experimental details are provided in the supplemental material, and Supplemental Schemes 1 and 2 summarize the GB2-Cy3 synthetic strategy (supplemental materials are available at http://jnm.snmjournals.org).

In Vivo Glucose Uptake Imaging

Wild-type zebrafish (*Danio rerio*) were maintained following the Canadian Council on Animal Care Guidelines. In vivo uptake of GB2-Cy3 was visualized in a zebrafish model by modifications of previous protocols (*23,30*). Full experimental details are provided in the supplemental material. This study was approved by the University of Windsor Animal Care Committee.

Statistical Analysis

Statistical analysis was done using GraphPad Prism. The results are expressed as the mean ± SEM. The box–whisker plots show the median (horizontal line), the interquartile range (margins of box), and the absolute range (vertical line). Differences between 2 groups were compared by unpaired Student *t* testing. One-way ANOVA was followed by a Benjamini–Hochberg or Tukey adjustment. Neurite length was measured by manual tracing and determined using National Institutes of Health ImageJ software as previously described (*11,31*). Pearson correlation was used for nearest-neighbor analysis and pairwise correlation of the studied genes. Kaplan–Meier plots and heat maps were generated using camcAPP (*32*) and Broad Institute Morpheus software.

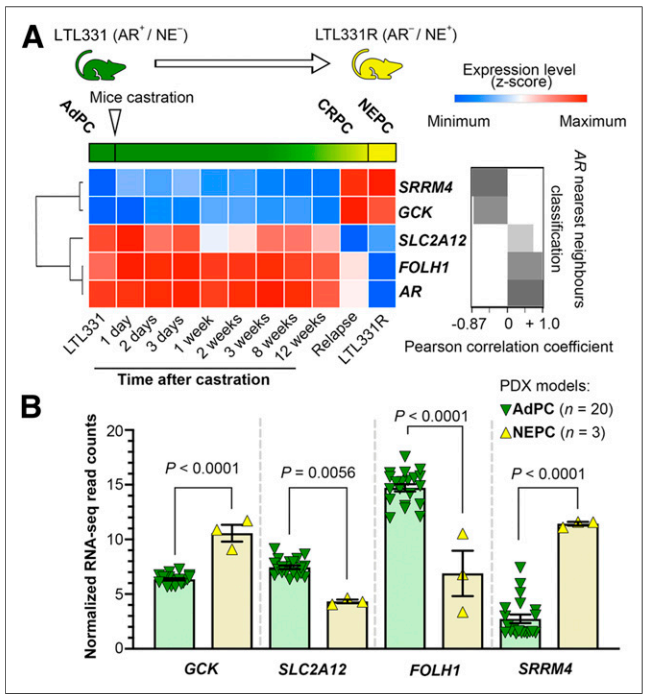

FIGURE 3. NEPC PDX models have suppressed expression of *FOLH1* and differential expressions of *SLC2A12* and *GCK*. (A) Transcription of studied genes during progression to NEPC and correlation with AR. (B) Expression of studied genes in PDX models.

RESULTS

Differential Expression of FOLH1, SLC2A, and Hexokinase in mCRPC

Figure 1A shows that expression of *SLC2A12* and *FOLH1* are the nearest neighbors to *AR* ($r > 0.6$, $P < 0.01$) and *GCK* is the farthest neighbor ($r = -0.6$, $P < 0.01$) in the UW cohort (*3*). We observed a significant suppression of *FOLH1* in low-AR mCRPC phenotypes, including NEPC and DNPC samples (Fig. 1B). Figure 1C shows that NEPC tumors have a 5-fold elevation of *GCK* ($P < 0.0001$) when compared with AR-positive samples. Alternatively, Figure 1D demonstrates that NEPC and DNPC samples suppress expression of *SLC2A12*. Supplemental Figure 1 verifies that in the Beltran cohort (*4*) *FOLH1*-suppressed NEPC samples have similar profiles of GLUT gene expression. In summary, *GCK* gene expression is elevated and the *SLC2A12* gene is suppressed in NEPC.

Differential Expression of SLC2A and Hexokinase in NELPC

The meta signature of prototypical high-grade NEPC (*25*) was used to isolate a potential NELPC group among a population of metastatic and primary AdPC samples lacking NEPC histopathology (Supplemental Figs. 2 and 3). Figure 2A shows that the transcriptionally identified NELPC subset had a shorter time to biochemical recurrence in NELPC (log-rank $P = 0.02$). Figure 2B shows a NELPC hallmark in both primary and metastatic samples, with the more prevalent signature seen in samples that are metastatic and have a high Gleason score. Figure 2C shows a lack of hallmarks of AR response in NELPC. Supplemental Figure 4 shows that *SLC2A1, SLC2A3–5, SLC2A9, SLC2A10, SLC2A12–14, HK1,* and *HK2* genes cluster with *REST*; these are herein referred to as *REST*-clustered genes. On the other hand, *SLC2A2, SLC2A6–8, SLC2A11, HK3,* and *CGK* cluster with *SRRM4* and other neuroendocrine-markers; these are herein referred to as *SRRM4*-clustered genes. Pairwise correlation with *SRRM4* expression is presented in Supplemental Figures 5–7. Similar to NEPC, *SLC2A12* and *FOLH1* expression is decreased in NELPC relative to AdPC (Fig. 2D). *GCK* expression is significantly higher in NELPC.

The Association of SLC2A and Hexokinase with Gleason Score and Biochemical Recurrence in NELPC

Supplemental Figures 8–10 depict expression levels of the studied genes during progression of AdPC based on Gleason score. Most *REST*-clustered *SLC2A* genes and hexokinases are either unchanged or suppressed at high Gleason scores, whereas *SRRM4*-clustered genes are significantly increased in samples with high Gleason scores. Kaplan–Meier survival curves studying high and low expression levels of the studied genes are represented in Supplemental Figures 11–13. The high expression of *SRRM4*-clustered genes such as *GCK* and *REST*-clustered gene *SLC2A1* (as an exception) is significantly associated with decreased biochemical recurrence (log-rank $P = 0.015$ for *GCK*). Interestingly, high levels of *REST*-clustered genes, including *SLC2A12,* are associated with a shorter time to biochemical recurrence (log-rank $P = 0.012$ for *SLC2A12*). Supplemental Table 1 summarizes the performed analysis on NELPC.

Sharing of SLC2A12 Suppression and GCK Overexpression Among NEPC and NELPC

RNA-sequencing data from 268 PC samples from the Memorial Sloan Kettering Cancer Center (*24*), Beltran (*4*), and UW (*3*) cohorts were used to stratify *SLC2A1–SLC2A14* and *HK1–HK4* genes into neuroendocrine-clustered and AdPC-clustered groups (Supplemental Fig. 14). The intersection between the clustered genes in different cohorts and inclusion of the most differentially expressed genes showed that *GCK* is the most highly expressed gene and *SLC2A12* is the most suppressed gene in samples with an NEGS.

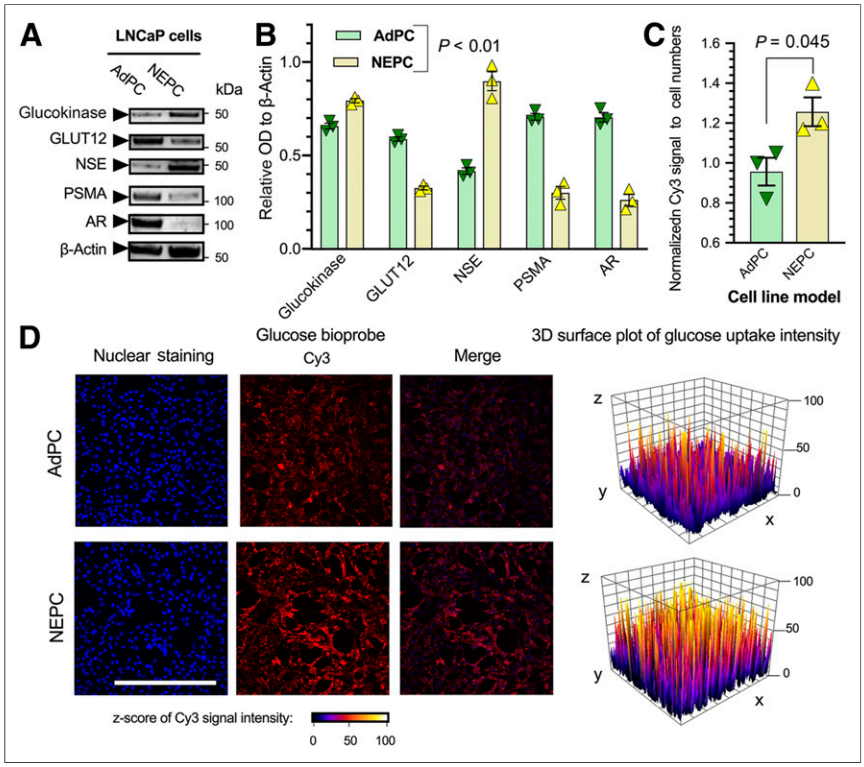

FIGURE 4. Neuroendocrine-induced LNCaP cell line represents higher glucose uptake and differential protein levels of glucokinase and GLUT12. (A and B) Western blot analyses of protein levels. (C and D) Quantification of GB2-Cy3 uptake and representative images of LNCaP cells. Scale bar = 200 μm.

The Distinct GCK-Amplified and SLC2A12-Suppressed Signature of NEPC in PDX Models

The LTL331 PDX is a model of PC progression from AdPC to NEPC. LTL331 tumors regress after castration but relapse within 24–32 mo with tumors harboring NEPC phenotypes (*27*). Figure 3A demonstrates that *GCK* expression is minimal before progression to CRPC but maximizes after cellular plasticity to CRPC and NEPC. Conversely, *SLC2A12* expression maximizes in hormone sensitive AdPC and, with a slight fluctuation, gradually decreases after castration. The expression of *SLC2A12* and *FOLH1* is the nearest neighbor to AR ($r > 0.6$, $P < 0.01$), and *GCK* is the farthest neighbor ($r = -0.87$, $P < 0.01$) in the UW cohort (*3*). Figure 3B shows—in our other well-characterized PDX models consisting of 20 AdPC and 3 NEPC models—that we observed significant elevation of *GCK* and suppression of *SLC2A12*

gene expression in the NEPC models. Overall, NEPC models have a *SLC2A12*-low and *GCK*-high signature.

Higher In Vitro and In Vivo Glucose Uptake in Neuroendocrine-Induced Cell Lines

To investigate the role of progression to a neuroendocrine phenotype on glucose uptake, we used the well-characterized neuroendocrine subclone cell line (LNCaP-NEPC) in which NEPC cells are derived from LNCaP cells (LNCaP-AdPC) by culturing in an androgen-depleted environment to mimic clinical androgen-deprivation therapy (Supplemental Figs. 15A, 15B, and 15D) (*33*). Figure 4A shows that protein levels of the neuroendocrine marker NSE are increased in the LNCaP-NEPC, whereas PSMA and AR levels are significantly decreased. The LNCaP-NEPC cell line has a significantly higher level of glucokinase (GCK) protein and a significantly lower level of GLUT12 (Fig. 4B).

Supplemental Figures 16–23 chemically characterize GB2-Cy3. Supplemental Figure 24 illustrates GB2-Cy3 uptake and its localization in LNCaP cells. Figure 4C shows that the LNCaP-NEPC cell line has a higher in vitro uptake of GB2-Cy3. Similarly, a zebrafish model was used for nonradioactive in vivo imaging of glucose uptake and displayed higher GB2-Cy3 in engrafted LNCaP-NEPC cells (Fig. 5). These observations indicate that suppression of PSMA and AR and elevation of neuroendocrine markers in LNCaP cell lines are associated with a differential level of glucose uptake, suppression of GLUT12, and elevation of glucokinase proteins.

DISCUSSION

The development of AR-indifferent and neuroendocrine-positive tumor phenotypes through divergent clonal evolution as a mechanism of resistance to AR inhibition in mCRPC is a well-characterized concept (*3,4*). However, Stelloo et al. (*2*) identified an NELPC in a treatment-naïve and primary cohort. Our work identified an NELPC subset among primary and metastatic samples with no history of exposure to next-generation AR inhibitors. Our data also show that the incidence of NELPC is more prevalent in metastatic specimens. These data support that either AR-indifferent subsets of cells can exist among AdPC that possess a greater susceptibility for neuroendocrine transdifferentiation or AR-indifferent, neuroendocrine-like cells exist from an early time point and are gradually selected for during treatment pressures.

Clinically, there are data to support a correlation between the detection rate of ^{68}Ga-PSMA-11 and the prostate-specific antigen level (*7*). Also, patients with low levels of prostate-specific antigen show lower PSMA-radioligand uptake and higher ^{18}F-FDG uptake (*18,20*). This relationship supports the goals of this study to investigate the mechanistic basis for ^{18}F-FDG avidity in NEPC and DNPC. Here, we show that the isoforms of GLUTs are structurally and functionally related proteins with different affinities to glucose. They are expressed in different cells on the basis of the metabolic necessity for glucose uptake (*34*). The elevation of glycolysis in NEPC has been previously reported (*35,36*). Irrespective of the overall contribution of GLUT to glucose metabolism, GLUT and hexokinase family members could be associated with ^{18}F-FDG uptake (*13,14*). Like glucose, ^{18}F-FDG is phosphorylated by hexokinases whereas their products, glucose-6-phosphate and FDG-6-phosphate, can have different levels of inhibition on hexokinases depending on their structure (*37*). Supplemental Figure 25 represents structural domains of the isoforms of human hexokinase proteins (*38*). Glucokinase lacks the N terminus domain and cannot be inhibited by either glucose-6-phosphate or FDG-6-phosphate.

GLUT11 is considered a high-affinity GLUT and can be effectual in elevation of glucose uptake while it is amplified (*34*). McBrayer et al. (*39*) evaluated the association of GLUT11 expression and ^{18}F-FDG uptake in multiple myeloma. We have observed a significant elevation of GLUT11 expression in both NEPC and NELPC. Similarly, GLUT7 and GLUT8 have a high affinity to glucose (*40*), and we observed their upregulation in samples with NEGS. Contrary to HK1–HK3, glucokinase, which is known as a glucose sensor in pancreatic β-cells, is not inhibited by its product glucose-6-phosphate but remains active while glucose is abundant (*37,38*). We can speculate that the apparent elevation of glucose uptake in NEPC or NELPC could be due to elevation of the expression of the aforementioned high affinity of GLUTs (Supplemental Fig. 26). Although our study provides functional support for this conclusion, it is also important to remember the complications associated with a focus on gene expression of this vast family of glucose transport regulators. Avril's commentary (*13*) elaborates on the complex number of molecule-, cell-, tissue-, and organ-related variables regulating the resulting ^{18}F-FDG signal, all of which may provide inconsistencies between GLUT expression and the resulting ^{18}F-FDG signal.

GLUT1 is a high-affinity and basal GLUT expressed ubiquitously in human tissues. In

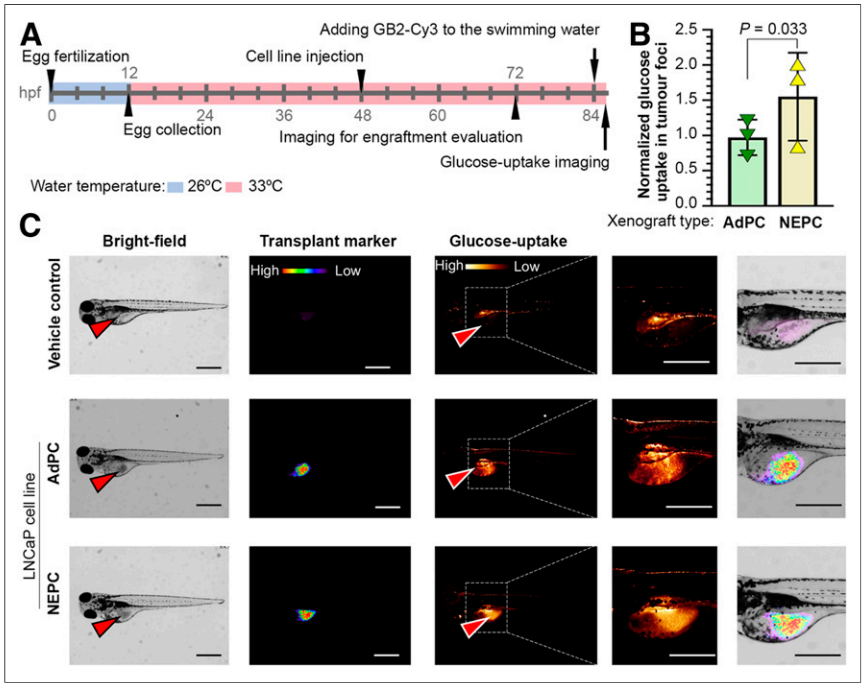

FIGURE 5. Neuroendocrine-induced LNCaP cell line xenografts represent higher glucose uptake in zebrafish model. (A) Schematic of experiment. (B and C) Quantification of GB2-Cy3 uptake and representative images of embryos injected with different LNCaP cells. Arrowheads show injection sites. Scale bar = 200 μm.

hormone-sensitive PC, GLUT1 gene expression positively correlates with androgen levels (*41*). Our work implies that GLUT1 expression has limited prognostic potential since it cannot estimate the development or existence of low-AR phenotypes such as NEPC or DNPC phenotype. GLUT12 has recently been introduced as a downstream target of AR, and its expression is tightly regulated by androgens (*42*). Our data demonstrated that the *SLC2A12* suppression is also highly associated with the development of a PSMA-low and neuroendocrine-high gene signature in mCRPC. This work shows that *GCK* upregulation and *SLC2A12* suppression correlate with the PSMA suppression, higher Gleason score, and shorter time to biochemical recurrence in NELPC.

For preclinical studies, the use of ^{18}F-FDG imaging in mouse xenografts can be limited by several factors, such as the operating cost and short half-life of the radioactive substance and nonradioactive glucose probes, which are of particular interest (*21*). Also, the engraftment of tumors in mice can be challenging to establish and is time consuming. This work demonstrates the feasibility of nonradioactive imaging of glucose uptake in PC xenografts using a zebrafish model as a rapid and cost-effective model.

CONCLUSION

NEPC, DNPC, and NELPC have distinct differential expression of GLUT and hexokinase genes. In accordance with this expression, the suppression of PSMA in NEPC is associated with elevated glucose uptake.

DISCLOSURE

This study was supported by the Canadian Institutes of Health Research (142189 [Lisa Porter] and PJT156150 [Xuesen Dong]), the Natural Sciences and Engineering Research Council of Canada (2018-06338 [John Trant]), and a grant from the Korea Health Technology R&D Project through the Korea Health Industry Development Institute (KHIDI), funded by the Ministry of Health and Welfare, Republic of Korea (H18C1916 [Gi Jeong Cheon]). Financial support was also provided by TELUS Ride for Dad, the PC Fight Foundation (Lisa Porter), and the Ontario Trillium Scholarship Program (Martin Bakht). The gene expression analysis was supported in part by a Department of Defense Idea Development Award-Partnering-PI (W81XWH-17-1-0414;W81XWH-17-1-0415 [Colm Morrissey]) and the Pacific Northwest PC SPORE (P50CA97186 [Colm Morrissey]). No other potential conflict of interest relevant to this article was reported.

KEY POINTS

QUESTION: Do the expression levels of glucose uptake–associated genes correlate with the development of NEGS or suppression of the PSMA gene?

PERTINENT FINDINGS: Data-mining approaches, cell lines, mouse, and zebrafish PDX models were used to demonstrate that GLUT and hexokinase expression, specially *GCK* and *SCL2A12,* is associated with NEGS, PSMA suppression, and higher glucose uptake.

IMPLICATIONS FOR PATIENT CARE: This study supports the use of ^{18}F-FDG PET for imaging of low-PSMA PC tumors with NEGS.

REFERENCES

1. Stelloo S, Bergman AM, Zwart W. Androgen receptor enhancer usage and the chromatin regulatory landscape in human prostate cancers. *Endocr Relat Cancer.* 2019;26:267–285.
2. Stelloo S, Nevedomskaya E, Kim Y, et al. Integrative epigenetic taxonomy of primary prostate cancer. *Nat Commun.* 2018;9:4900.
3. Bluemn EG, Coleman IM, Lucas JM, et al. Androgen receptor pathway-independent prostate cancer is sustained through FGF signaling. *Cancer Cell.* 2017;32:474–489.e6.
4. Beltran H, Prandi D, Mosquera JM, et al. Divergent clonal evolution of castration resistant neuroendocrine prostate cancer. *Nat Med.* 2016;22:298–305.
5. Alshalalfa M, Liu Y, Wyatt AW, et al. Characterization of transcriptomic signature of primary prostate cancer analogous to prostatic small cell neuroendocrine carcinoma. *Int J Cancer.* 2019;145:3453–3461.
6. Li Y, Donmez N, Sahinalp C, et al. SRRM4 drives neuroendocrine transdifferentiation of prostate adenocarcinoma under androgen receptor pathway inhibition. *Eur Urol.* 2017;71:68–78.
7. Hope TA, Goodman JZ, Allen IE, et al. Meta-analysis of ^{68}Ga-PSMA-11 PET accuracy for the detection of prostate cancer validated by histopathology. *J Nucl Med.* 2019;60:786–793.
8. Sheikhbahaei S, Afshar-Oromieh A, Eiber M, et al. Pearls and pitfalls in clinical interpretation of prostate-specific membrane antigen (PSMA)-targeted PET imaging. *Eur J Nucl Med Mol Imaging.* 2017;44:2117–2136.
9. Tosoian JJ, Gorin MA, Rowe SP, et al. Correlation of PSMA-targeted ^{18}F-DCFPyL PET/CT findings with immunohistochemical and genomic data in a patient with metastatic neuroendocrine prostate cancer. *Clin Genitourin Cancer.* 2017;15:e65–e68.
10. Chakraborty PS, Tripathi M, Agarwal KK, et al. Metastatic poorly differentiated prostatic carcinoma with neuroendocrine differentiation: negative on ^{68}Ga-PSMA PET/CT. *Clin Nucl Med.* 2015;40:e163–e166.
11. Bakht MK, Derecichei I, Li Y, et al. Neuroendocrine differentiation of prostate cancer leads to PSMA suppression. *Endocr Relat Cancer.* 2018;26:131–146.
12. Haberkorn U, Ziegler SI, Oberdorfer F, et al. FDG uptake, tumor proliferation and expression of glycolysis associated genes in animal tumor models. *Nucl Med Biol.* 1994;21:827–834.
13. Avril N. GLUT1 expression in tissue and ^{18}F-FDG uptake. *J Nucl Med.* 2004;45:930–932.
14. Yang H, Zhong JT, Zhou SH, Han HM. Roles of GLUT-1 and HK-II expression in the biological behavior of head and neck cancer. *Oncotarget.* 2019;10:3066–3083.
15. Bozkurt MF, Virgolini I, Balogova S, et al. Guideline for PET/CT imaging of neuroendocrine neoplasms with ^{68}Ga-DOTA-conjugated somatostatin receptor targeting peptides and ^{18}F–DOPA. *Eur J Nucl Med Mol Imaging.* 2017;44:1588–1601.
16. Jadvar H. PET of glucose metabolism and cellular proliferation in prostate cancer. *J Nucl Med.* 2016;57(suppl):25S–29S.
17. Perez PM, Hope TA, Behr SC, et al. Intertumoral heterogeneity of ^{18}F-FDG and ^{68}Ga-PSMA uptake in prostate cancer pulmonary metastases. *Clin Nucl Med.* 2019;44:e28–e32.
18. Parida GK, Tripathy S, Datta Gupta S, et al. Adenocarcinoma prostate with neuroendocrine differentiation: potential utility of ^{18}F-FDG PET/CT and ^{68}Ga-DOTANOC PET/CT over ^{68}Ga-PSMA PET/CT. *Clin Nucl Med.* 2018;43:248–249.
19. Spratt DE, Gavane S, Tarlinton L, et al. Utility of FDG-PET in clinical neuroendocrine prostate cancer. *Prostate.* 2014;74:1153–1159.
20. Thang SP, Violet J, Sandhu S, et al. Poor outcomes for patients with metastatic castration-resistant prostate cancer with low prostate-specific membrane antigen (PSMA) expression deemed ineligible for ^{177}Lu-labelled PSMA radioligand therapy. *Eur Urol Oncol.* 2019;2:670–676.
21. Cheng Z, Levi J, Xiong Z, et al. Near-infrared fluorescent deoxyglucose analogue for tumor optical imaging in cell culture and living mice. *Bioconjug Chem.* 2006;17:662–669.
22. Lee HY, Lee JJ, Park J, Park SB. Development of fluorescent glucose bioprobes and their application on real-time and quantitative monitoring of glucose uptake in living cells. *Chemistry.* 2011;17:143–150.
23. Melong N, Steele S, MacDonald M, et al. Enzalutamide inhibits testosterone-induced growth of human prostate cancer xenografts in zebrafish and can induce bradycardia. *Sci Rep.* 2017;7:14698.
24. Taylor BS, Schultz N, Hieronymus H, et al. Integrative genomic profiling of human prostate cancer. *Cancer Cell.* 2010;18:11–22.
25. Tsai HK, Lehrer J, Alshalalfa M, Erho N, Davicioni E, Lotan TL. Gene expression signatures of neuroendocrine prostate cancer and primary small cell prostatic carcinoma. *BMC Cancer.* 2017;17:759.
26. Subramanian A, Tamayo P, Mootha VK, et al. Gene set enrichment analysis: a knowledge-based approach for interpreting genome-wide expression profiles. *Proc Natl Acad Sci USA.* 2005;102:15545–15550.
27. Akamatsu S, Wyatt AW, Lin D, et al. The placental gene PEG10 promotes progression of neuroendocrine prostate cancer. *Cell Reports.* 2015;12:922–936.

28. Korbel GA, Lalic G, Shair MD. Reaction microarrays: a method for rapidly determining the enantiomeric excess of thousands of samples. *J Am Chem Soc.* 2001;123:361–362.
29. Park J, Lee HY, Cho MH, Park SB. Development of a Cy3-labeled glucose bioprobe and its application in bioimaging and screening for anticancer agents. *Angew Chem Int Ed Engl.* 2007;46:2018–2022.
30. Park J, Um JI, Jo A, et al. Impact of molecular charge on GLUT-specific cellular uptake of glucose bioprobes and in vivo application of the glucose bioprobe, GB2-Cy3. *Chem Commun (Camb).* 2014;50:9251–9254.
31. Ding Y, Li Y, Lu L, et al. Inhibition of nischarin expression promotes neurite outgrowth through regulation of PAK activity. *PLoS One.* 2015;10:e0144948.
32. Dunning MJ, Vowler SL, Lalonde E, et al. Mining human prostate cancer datasets: the "camcAPP" Shiny app. *EBioMedicine.* 2017;17:5–6.
33. Yuan T-C, Veeramani S, Lin F-F, et al. Androgen deprivation induces human prostate epithelial neuroendocrine differentiation of androgen-sensitive LNCaP cells. *Endocr Relat Cancer.* 2006;13:151–167.
34. Qian Y, Wang X, Chen X. Inhibitors of glucose transport and glycolysis as novel anticancer therapeutics. *World J Transl Med.* 2014;3:37–57.
35. Choi SYC, Ettinger SL, Lin D, et al. Targeting MCT 4 to reduce lactic acid secretion and glycolysis for treatment of neuroendocrine prostate cancer. *Cancer Med.* 2018;7:3385–3392.
36. Li W, Cohen A, Sun Y, et al. The role of CD44 in glucose metabolism in prostatic small cell neuroendocrine carcinoma. *Mol Cancer Res.* 2016;14:344–353.
37. McKerrecher D, Waring MJ. Property-based design in the optimisation of benzamide glucokinase activators—from hit to clinic. *Prog Med Chem.* 2013;52:1–43.
38. Roberts DJ, Miyamoto S. Hexokinase II integrates energy metabolism and cellular protection: akting on mitochondria and TORCing to autophagy. *Cell Death Differ.* 2015;22:364.
39. McBrayer SK, Cheng JC, Singhal S, Krett NL, Rosen ST, Shanmugam M. Multiple myeloma exhibits novel dependence on GLUT4, GLUT8, and GLUT11: implications for glucose transporter-directed therapy. *Blood.* 2012;119:4686–4697.
40. Gonzalez-Menendez P, Hevia D, Mayo JC, Sainz RM. The dark side of glucose transporters in prostate cancer: are they a new feature to characterize carcinomas? *Int J Cancer.* 2018;142:2414–2424.
41. Vaz CV, Marques R, Alves MG, et al. Androgens enhance the glycolytic metabolism and lactate export in prostate cancer cells by modulating the expression of GLUT1, GLUT3, PFK, LDH and MCT4 genes. *J Cancer Res Clin Oncol.* 2016;142:5–16.
42. White MA, Tsouko E, Lin C, et al. GLUT12 promotes prostate cancer cell growth and is regulated by androgens and CaMKK2 signaling. *Endocr Relat Cancer.* 2018;25:453–469.

The Journal of NUCLEAR MEDICINE

Differential Expression of Glucose Transporters and Hexokinases in Prostate Cancer with a Neuroendocrine Gene Signature: A Mechanistic Perspective for ^{18}F-FDG Imaging of PSMA-Suppressed Tumors

Martin K. Bakht, Jessica M. Lovnicki, Janice Tubman, Keith F. Stringer, Jonathan Chiaramonte, Michael R. Reynolds, Iulian Derecichei, Rosa-Maria Ferraiuolo, Bre-Anne Fifield, Dorota Lubanska, So Won Oh, Gi Jeong Cheon, Cheol Kwak, Chang Wook Jeong, Keon Wook Kang, John F. Trant, Colm Morrissey, Ilsa M. Coleman, Yuzhuo Wang, Hojjat Ahmadzadehfar, Xuesen Dong and Lisa A. Porter

J Nucl Med. 2020;61:904-910.
Published online: December 5, 2019.
Doi: 10.2967/jnumed.119.231068

The Journal of Nuclear Medicine is published monthly.
SNMMI | Society of Nuclear Medicine and Molecular Imaging
1850 Samuel Morse Drive, Reston, VA 20190.
(Print ISSN: 0161-5505, Online ISSN: 2159-662X)

SNMMI SOCIETY OF NUCLEAR MEDICINE AND MOLECULAR IMAGING